Vibration-based bearing fault detection on experimental wind turbine gearbox data

Cédric Peeters[1], Patrick Guillaume[2], and Jan Helsen[3]

[1,2,3] *University of Brussels - VUB, Faculty of Mechanical Engineering, Elsene, Brussels, 1050, Belgium*
Cedric.Peeters@vub.ac.be
Patrick.Guillaume@vub.ac.be
jahelsen@vub.ac.be

ABSTRACT

Rolling element bearing faults are one of the most common defects in rotating machinery. The detection of these faults has lately attracted an increasing amount of attention in the industry. Detecting the faults in their incipient phase can prevent a more catastrophic breakdown of a machine and can save a company time and money. An often occurring problem in analyzing vibration measurements of a rotating machine is the presence of harmonic signal components originating from different machine parts. This paper focuses on separating the bearing fault signals from other masking signal content coming from elements like gears or rotating shafts. The separation is based on the assumption that signal components of gears or shafts are deterministic and appear as clear peaks in the frequency spectrum, whereas bearing signals are stochastic due to random jitter on their fundamental period and can be classified as cyclostationary. A technique that has recently gained more attention for separating these two types of signals is the cepstral editing procedure (CEP). This preprocessing method is investigated further in this paper as an automated procedure. The cepstral editing procedure makes use of the fact that deterministic components appear in the cepstrum as narrow peaks and removal of these cepstral peaks reduces the amplitude of the corresponding discrete components. The residual stochastic signal after cepstral editing should consist mainly out of bearing fault signals in certain frequency bands. To analyze the residual signal the squared envelope spectrum is examined. The issue of selecting the proper frequency band where to demodulate the signal necessary for enveloping is addressed through the use of spectral kurtosis. The performance of the developed methods will be validated on experimental data from the National Renewable Energy Laboratory (NREL). This data has been made available by NREL in the context of the wind turbine gearbox condition monitoring round robin study. As such other research teams from around the world have analyzed this data as well and published their findings. The measurements were done on a wind turbine gearbox in a healthy and damaged condition and the setup is documented extensively, making it well suited for a performance comparison. A summary of the findings on the NREL data is discussed in this paper.

1. INTRODUCTION

Rolling element bearings are one of the most widely used machine elements in rotating machinery. It is estimated that more than 90% of rotating machines (Graney & Starry, 2012) contain this type of bearings. Unfortunately, they are susceptible to a multitude of premature deficiencies and less than 10% of rolling element bearings (A.I.Technologies, 2009) reach their expected basic L10 life, the life at which ten percent of the bearings can be expected to have failed due to normal fatigue failure for that particular application. These observations imply a need for an improved comprehensive condition-based maintenance program.

However there are still some hurdles to be overcome before such an exhaustive program becomes fully feasible. One of these problems is the detection of characteristic bearing fault frequencies that are masked by high energy harmonic signals originating from other machine elements like shafts or gears. Separating the bearing fault signals from other masking signal content of such elements is thus a valuable endeavor. The separation is based on the assumption that bearing fault signals are stochastic due to random jitter on their fundamental period and can be categorized as cyclostationary whereas gear or shaft signals are deterministic and appear as distinct peaks in the amplitude spectrum (Antoni & Randall, 2003).

Recently there have been a number of developments concerning the topic of discrete components removal (DCR). Examples of such preprocessing techniques include time-synchronous averaging (TSA) (McFadden & Toozhy, 2000), self-adaptive noise cancellation (SANC)(Antoni & Randall, 2004a), lin-

ear prediction filtering (LPF) (Sawalhi & Randall, 2004), discrete/random separation (DRS)(Antoni & Randall, 2004b) and cepstral editing (CEP) (R. B. Randall & Sawalhi, 2014). This last preprocessing technique is investigated further in this paper as it shows great potential in separating cyclostationary bearing signals from discrete components (Ompusunggu, n.d.). Qualitative studies by (Kilundu, Ompusunggu, Elasha, & Mba, 2014) and (R. Randall, Sawalhi, & Coats, 2011) have been conducted comparing cepstral editing to the other aforementioned methods. These studies indicated through experimental tests that the CEP technique can outperform the other methods.

The ambition of this paper is to validate the performance of the cepstrum editing procedure by applying it to the well-documented experimental vibration data, provided by the *National Renewable Energy Laboratory* in light of a past *wind turbine gearbox condition monitoring round robin study*.

2. CEPSTRUM EDITING PROCEDURE

2.1. The cepstrum

Recently the attention for using the cepstrum in vibration-based condition monitoring has increased significantly. Where in the past the main use of the cepstrum was the detection of echos in speech or seismic signals (R. B. Randall, 2013), it is now realized that the cepstrum can be applied as well to the problem of discrete and random component separation for vibration signals.

Throughout history, there have been various definitions and discussions of the cepstrum of a signal (Bogert, Healy, & Tukey, 1963; Childers, Skinner, & Kemerait, 1977; Polydoros & Fam, 1981; R. Randall & Hee, 1982; Antoni, Daniere, & Guillet, 2000), the definitions used in this paper, however, are described as the complex and real cepstrum. The real cepstrum has proven to be effective for achieving edited time signals by editing the logarithmic amplitude spectrum of stationary signals without having to fiddle with the phase.

Mathematically the complex cepstrum can be written as the inverse Fourier transform of the log spectrum, which is expressed in terms of the amplitude and phase:

$$C_c(\tau) = \mathscr{F}^{-1}\{log(X(f))\} = \mathscr{F}^{-1}\{ln(A(f)) + j\phi(f)\} \tag{1}$$

where $X(f)$ is the frequency spectrum of the signal $x(t)$:

$$X(f) = \mathscr{F}\{x(t)\} = A(f)e^{j\phi(f)}. \tag{2}$$

By setting the phase to zero in Eq.(1), the real cepstrum can be obtained:

$$C_r(\tau) = \mathscr{F}^{-1}\{ln(A(f))\}. \tag{3}$$

In Eq. (3) τ is referred to as *"quefrency"* and can be seen as a type of time-domain index. Harmonic components with a period h_0 in a signal correspond to a peak in the cepstrum at quefrency h_0.

2.2. Cepstral editing

The cepstrum has the interesting property that it is able to concentrate periodic spectral components (e.g. harmonics) into a smaller number of impulses called *"rahmonics"*. Removal of these peaks, also called *"liftering"*, corresponds to a decrease of the log amplitude of the periodic components in the signal. The complex cepstrum contains both amplitude and phase information which enables reversing back to time domain after editing, but in order to calculate the complex cepstrum the phase needs to be unwrapped. This is undesirable for stationary signals consisting of discrete frequency components, where the phase is undefined at intermediate frequencies (Dalpiaz et al., 2013).

However, it was recently shown by (R. B. Randall & Sawalhi, 2011) that the real cepstrum is a more effective way of editing the log amplitude spectrum of signals containing harmonic components. Recombining this edited amplitude spectrum with the original phase produces the edited time domain signal. This cepstrum editing procedure (CEP) has been further investigated by (Sawalhi & Randall, 2011; Borghesani, Pennacchi, Randall, Sawalhi, & Ricci, 2013; R. B. Randall & Sawalhi, 2014) where it was shown that the CEP method is a simple method to implement for separating deterministic signal content from random or cyclostationary signal content. While the editing of certain frequencies introduces some phase distortion, this is generally negligible compared to the significant reduction in amplitude at those frequencies. A general scheme of the CEP method is shown in Fig.1. It can be seen that the most crucial part in the CEP method is the editing of the real cepstrum. To enhance the applicability of the CEP method to industrial environments, an automated editing procedure is used in this paper instead of a manual one. It has been shown by (Ompusunggu, n.d.) that it is possible to implement a robust and efficient automated liftering of the harmonic signal content.

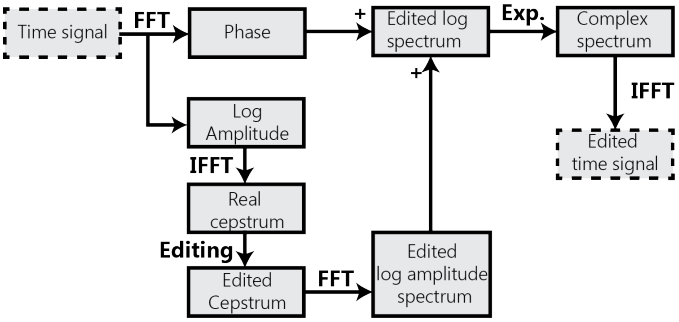

Figure 1. Schematic diagram of the cepstrum editing procedure.

2.3. Automated cepstrum editing procedure (ACEP)

In order to replace the manual procedure by an automated one, there needs to be a more intelligent automated cepstral peak selection. Figure 2 displays an overview of the steps to automate the editing. It can be seen that the real cepstrum is enhanced before the actual peak selection. The reason for the enhancement is simply to make the peak detection step easier and more straightforward. First, the cepstrum is long-pass liftered as to prevent liftering of low quefrency content. Second, a wavelet denoising and spectral subtraction (SS) method is used to reduce the amount of noise present in the signal. Afterwards, a notch lifter is generated based on the automatic peak detection on the denoised cepstrum. Lastly, the original real cepstrum is liftered with the resulting notch lifter.

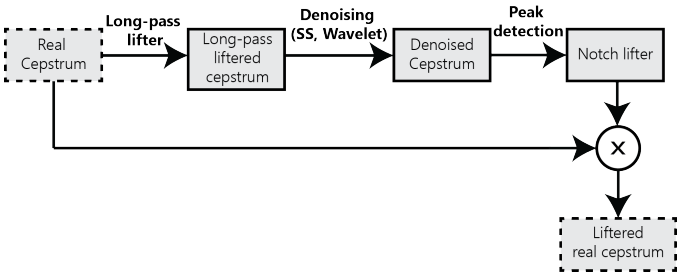

Figure 2. Schematic diagram of the automated cepstrum editing step.

2.3.1. Long-pass lifter

Transforming the signal to the cepstral domain leads to a concentration of modal information in the low quefrency region. After the ACEP method however, the signal is band-pass filtered before envelope analysis, making it preferable to retain the system resonances. Thus, the low quefrency region is liftered away before the notch lifter generation step, implying that there will be no detected peaks corresponding to modal content.

For a general case it is difficult to determine the appropriate cut-off quefrency. The decision can be based on the resonance frequencies that are present in the investigated system, but this involves manual inspection of the signal. To automate the procedure, it is reasonable to construct a long-pass lifter with a relatively high cut-off quefrency as to have a safety margin and to prevent liftering away too much modal content. A user should take into account the type and size of the machine on which they perform the analysis.

If $n, N_{cut-off}$ and L are respectively the sample quefrency index, the cut-off quefrency index and the sample length of the cepstrum, the long-pass lifter can be defined as follows:

$$l_{LP}(n) = \begin{cases} 0 & n = 1 : N_{cut-off} \\ 1 & n = N_{cut-off} + 1 : L \end{cases} \tag{4}$$

Applying the lifter to the unedited real cepstrum $c(n)$ produces the long-pass liftered cepstrum:

$$c_{LP}(n) = c(n) l_{LP}(n). \tag{5}$$

2.3.2. Noise reduction

After the long-pass filtering step, the cepstrum is denoised using two conventional denoising methods. As proposed by (Ompusunggu, n.d.), the first applied method is spectral subtraction (SS). To smooth the cepstrum further, wavelet denoising is used afterwards.

Spectral subtraction

The spectral subtraction method was originally introduced by (Boll, 1979) as an acoustic speech enhancement technique and later an ample amount of variations have been developed (Martin, 1994; Lebart, Boucher, & Denbigh, 2001). In this paper the multi-band spectral subtraction proposed by (Kamath & Loizou, 2002) is used.

The spectral subtraction method estimates the noise spectrum and the average signal spectrum and then subtracts them from each other, improving the average signal-to-noise ratio (SNR). Usually noise is coloured and not perfect white Gaussian noise. The multi-band spectral subtraction method allows to some degree the presence of coloured noise because the filtering of the signal spectrum is separated into different frequency bands.

Being a transformation of the measured time signal, the cepstrum contains noise as well and can be regarded as an addition of discrete signal components $\tilde{c}(n)$ and noise $d(n)$:

$$c_{LP}(n) = \tilde{c}(n) + d(n). \tag{6}$$

A diagram of the multi-band spectral subtraction technique is shown in Fig.3. The SS technique makes use of a window basis for calculating the Fourier transform and performing the denoising procedure. The amplitude $|C(f,k)|$ is employed for estimating the average noise spectrum in every frequency band iteratively. The estimated amplitude $|\tilde{C}(f,k)|$ is obtained by subtracting the noise estimate from the original amplitude $|C(f,k)|$. Finally, the de-noised cepstrum $\tilde{c}(n)$ is reconstructed using the original phase $\angle C(f,k)$ and the amplitude estimates of all window frames.

Wavelet denoising

One of the primary applications of wavelets is denoising of signals. Wavelets allows for denoising in both time and frequency domain simultaneously and has even been used before as standalone method for bearing fault detection (R. B. Randall, 2011). Wavelet denoising employ thresholding methods where the wavelet coefficients are thresholded to remove

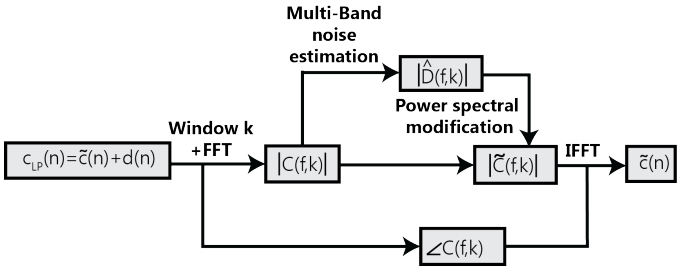

Figure 3. Schematic diagram of the multi-band spectral subtraction method.

the noisy signal content and is mostly based on research conducted by (Donoho & Johnstone, 1994). A 'hard thresholding' method leaves the retained coefficients unchanged, while a 'soft thresholding' method, as is used for the cepstrum, subtracts the noise estimate (threshold value) from the retained coefficients. The wavelet denoising method described here makes use of Daubechies3 wavelets and of universal thresholding. This paper doesn't go further into detail about the used wavelet denoising method however. For more information on wavelet denoising, the interested reader is referred to Refs.(Pasti, Walczak, Massart, & Reschiglian, 1999; R. B. Randall, 2011; Cohen, 2012).

2.3.3. Peak detection

After long-pass liftering and denoising, a fixed threshold of three standard deviations (3σ) is calculated from the residual cepstrum $c_r(n)$ as follows:

$$threshold = E[c_r(n)] + 3 \times std[c_r(n)], \tag{7}$$

where $E[.]$ and $std[.]$ denote respectively the expectation operator and the standard deviation operator. A vector m is constructed, based on all values greater than the threshold, containing all the corresponding sample indices:

$$m = \{\forall n | c_r(n) > threshold\} \tag{8}$$

While periodic signal components show up as sharp peaks in the cepstrum, second order cyclostationary components like bearing faults do not show up as a strong peak in the real cepstrum and thus they will not be detected nor liftered away.

2.3.4. Liftering

The final editing step is the generation of the notch lifter, based on the cepstral peaks of the denoised cepstrum, and the actual liftering of the unaltered real cepstrum with this lifter. It should be noted however that the notch width has a significant influence on the performance of the ACEP method. If there is speed variation present in the signal, it can be desirable to choose a larger notch width, but it shouldn't be chosen too large either since this can lead to excessively distorting the amplitude spectrum.

3. ADDITIONAL TECHNIQUES

While the goal of the ACEP method is to separate the signal into deterministic and stochastic components, there is still a need for other processing tools to be able to adequately diagnose the system. Thus three other techniques are used in addition to ACEP.

Order tracking
In order to properly analyse the signals and to account for speed variation, the data needs to be transformed from the time domain to the angular domain. Since the signals are sampled asynchronously with a constant sample rate, it is necessary to resample the signal at constant angular increments of a reference shaft. Usually this is done based on velocity measurements from a tachometer, which can be used to estimate the angular shaft position.

Band-pass filtering based on kurtosis
After the signal has been separated into deterministic and stochastic components, the residual signal can be demodulated for analysis of the envelope spectrum. However the choice of the proper demodulation band is often not a straightforward task. This paper makes use of spectral kurtosis to identify appropriate frequency bands for demodulation. More in particular the Kurtogram, developed by Jérôme Antoni (Antoni, 2007), is utilized to visually determine frequency bands with high kurtosis values.

Envelope analysis
Local faults in rolling element bearings produce impacts that are periodic with the corresponding characteristic frequency. However, in reality there is some jitter on this fundamental period, which makes higher order harmonics spread out. Lower order harmonics are usually masked by other background vibrations of gears or shafts. One of the most used techniques to circumvent this problem for bearing fault diagnosis is the analysis of the envelope spectrum. By analysing the spectrum of the envelope of the time signal, the information of interest incorporates the repetition frequency of the impacts. For further information, it is possible to find quite a few papers on the topic of envelope analysis (Courrech & Gaudet, 1998; Ho & Randall, 2000; R. B. Randall, Antoni, & Chobsaard, 2001).

4. EXPERIMENTAL APPLICATION

In order to test the performance of the developed methods, experimental data of a wind turbine from the National Renewable Energy Laboratory (NREL) will be used for validation and the results are compared to those summarized in (Sheng, 2012). The NREL dynamometer test facility (DTF) was used

for the data collection.

4.1. Description of experimental setup

Turbine

As can be seen on Fig.4(a), the test turbine is a three-bladed, stall-controlled, upwind turbine. It has a rated power of 750kW and the generator normally operates at 1800 rpm or 1200 rpm nominal. The complete drivetrain was installed in the NREL DTF as shown on Fig.4(b). It was hard fixed to the floor and missed the hub, rotor, yaw bearing and yaw drives.

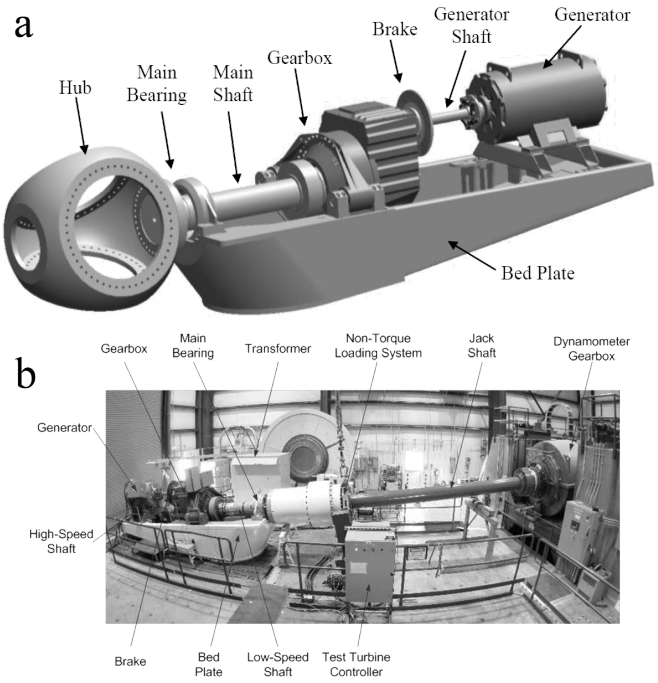

Figure 4. (a) Drive train configuration of the test turbine. (b) NREL dynamometer test stand with the turbine installed.

Gearbox

Two gearboxes of the same design were used for collecting the data, one in "healthy" state and the other one in "damaged" state. An exploded view of the gearbox is shown in Fig.5(a). The accelerometer vibration measurements along with high-speed shaft RPM data was made available. The "healthy" gearbox was only tested in the dynamometer while the "damaged" gearbox did a run-in first in the dynamometer and was later sent to a wind farm for field testing. Two loss-of-oil events damaged its internal bearings and gears. Afterwards, it was again installed in the dynamometer facility and retested in a controlled environment. The gearboxes consist of one low speed (LS) planetary stage and two parallel stages. The used nomenclature is the same as the one used by (Sheng, 2012) and can be seen in Fig.5(b).

Bearings

Various bearing types are used in the gearboxes corresponding to the loading conditions and life requirements. Two full-complement cylindrical roller bearings (fcCRB) support the planet carrier and two cylindrical roller bearings (CRB) support the planet gears. The parallel shafts are each supported by a CRB on the upwind side and by two tapered roller bearings (TRB) on the downwind side of the assembly. A list of all bearing locations, manufacturers, part numbers and types can be found in Table 1 and Fig.6 illustrates the locations and used names of the different bearings. If the component is positioned upwind, this is denoted with an 'A' and if it is downwind, with a 'B' or a 'C'. A full list of the gear and bearing characteristic frequencies is not given but can be determined based on Table 1.

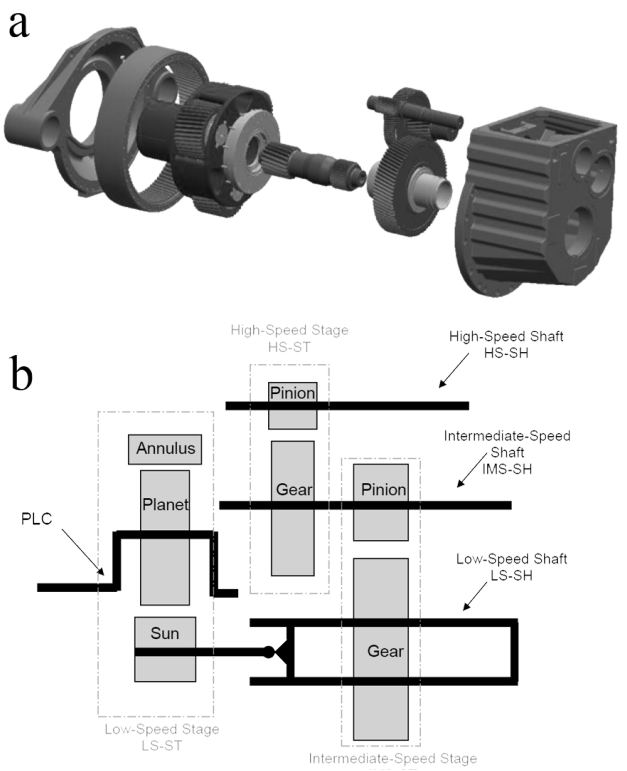

Figure 5. (a) View of internal components of the test gearbox. (b) Internal nomenclature and abbreviations of the test gearbox.

4.2. Measurement settings

The accelerometers were mounted on the outside of the gearbox and data was sampled at 40 kHz per channel. In total data sets of eight accelerometers (Model: IMI 626B02) were made available and the exact locations can be seen in Fig. 7. Lastly, Table 2 gives a summary of the signal names and their corresponding locations of the different vibration sensors.

Table 1. Overview of used bearing types, numbers and locations.

Location	Location designation	Type	Provider	Part number
Planet carrier	PLC-A	fcCRB	INA	SL181892E
	PLC-B	fcCRB	INA	SL 18 1880 72/K10
Planet	PL-A	CRB	FAG	NJ2232E.M1
	PL-B	CRB	FAG	NJ2232E.M1
Low-speed shaft	LS-SH-A	fcCRB	INA	SL181856E
	LS-SH-B	TRB	SKF	32948*
	LS-SH-C	TRB	SKF	32948*
Intermediate-speed shaft	IMS-SH-A	CRB	FAG	NU2220E.M1
	IMS-SH-B	TRB	SKF	32032 X
	IMS-SH-C	TRB	SKF	32032 X
High-speed shaft	HS-SH-A	CRB	FAG	NU2220E.M1
	HS-SH-B	TRB	SKF	32222 J2
	HS-SH-C	TRB	SKF	32222 J2

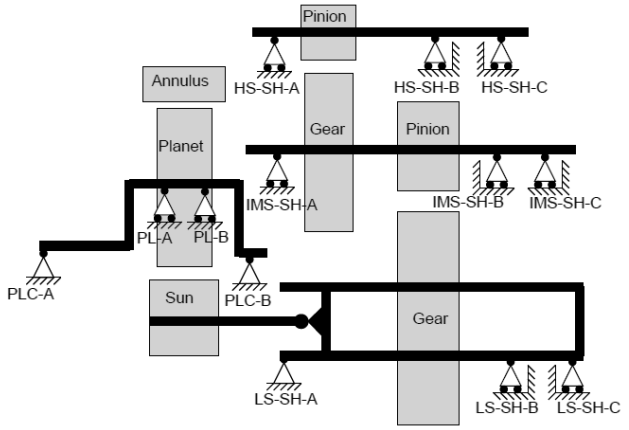

Figure 6. Locations and nomenclature of the bearings in the test gearbox.

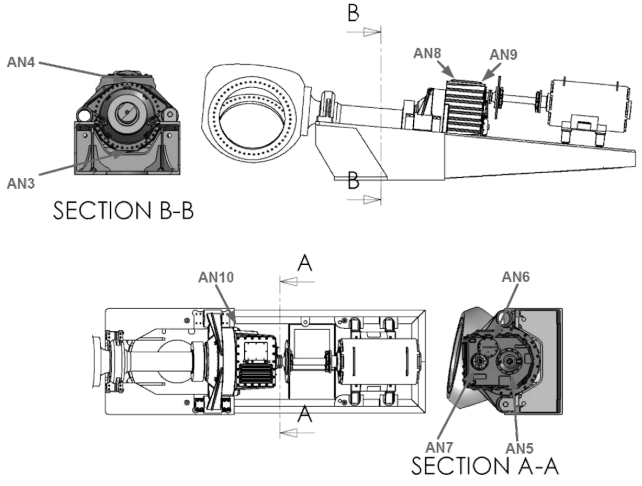

Figure 7. Overview of the accelerometer locations.

Table 2. List of the used sensors and their corresponding placement descriptions.

Sensor label	Location description
AN3	Ring gear radial 6 o'clock
AN4	Ring gear radial 12 oclock
AN5	LS-SH radial
AN6	IMS-SH radial
AN7	HS-SH radial
AN8	HS-SH upwind bearing radial
AN9	HS-SH downwind bearing radial
AN10	Carrier downwind radial

Table 3. Actual gearbox damage that should be detectable through vibration analysis.

Damage #	Component	Mode
1	HS-ST gear set	Scuffing
2	HS-SH downwind bearings	Overheating
3	IMS-ST gear set	Fretting corrosion, scuffing, polishing wear
4	IMS-SH upwind bearing	Assembly damage, scuffing, dents
5	IMS-SH downwind bearings	Assembly damage, dents
6	Annulus/ring gear, or sun pinion	Scuffing and polishing, fretting corrosion
7	Planet carrier upwind bearing	Fretting corrosion

4.3. Performance analysis

In order to assess the performance of the developed methods for bearing fault detection, the provided signals at 1800 rpm from the NREL test setup are investigated using a combination of the above-mentioned techniques. This results in four basic steps:

1. Order tracking
2. Automated cepstral editing
3. Band-pass filtering based on kurtosis
4. Squared envelope analysis

According the report of (Sheng, 2012), the research partners of the *Wind Turbine Gearbox Condition Monitoring Round Robin Study* agreed to a total of seven damages that were considered to be detectable through vibration analysis. Table 3 shows a summary of the detectable gearbox damage.

Since this paper focuses on bearing fault detection, no attention is given to the gear faults, meaning that four bearing faults are investigated. For each bearing the characteristic frequencies corresponding to the damages are shown in Table 4.

Table 4. Damaged bearings and their corresponding theoretical characteristic frequencies. *(BPFO: Ball Pass Frequency Outer race, BPFI: Ball Pass Frequency Inner race, FTF: Fundamental Train Frequency)*

Bearing label	Fault type	Detectable characteristic frequency [Hz]
HS-SH downwind bearings (*HSS-B& C*)	BPFI FTF	345,29Hz 12,75 Hz
IMS-SH downwind bearings (*ISS-B& C*)	BPFO	105,75 Hz
Planet carrier upwind bearing (*PLC-A*)	BPFO	8,81 Hz
IMS-SH upwind bearing (*ISS-A*)	BPFI	73,7 Hz

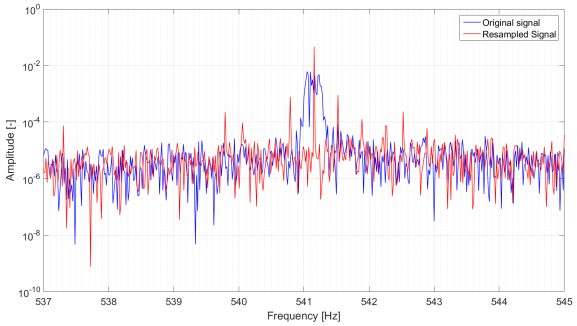

Figure 8. Zoom of the 18th harmonic of the 30 Hz shaft speed, measured by the AN7 sensor, before and after resampling.

4.3.1. Results

The bearing faults present in the system are spatially distributed over the gearbox, meaning that some sensors will be more likely to detect possible faults than others due to being in closer proximity to the source. To illustrate this and the used processing steps, the signal measured by sensor AN7 is analysed. This sensor is located near the high-speed shaft bearings, so it is expected that it should contain prominent signal content originating from the BPFI and FTF faults described in Table 4.

High-speed downwind bearings

The first step in the processing scheme is to resample the healthy and the damaged data so the speed variation present in the measurements is neutralized. Using the provided tacho signal and RPM measurements, all the signals are order tracked to provide a more accurate view on the frequencies present in the data. Figure 8 shows a zoomed picture of the 18th shaft speed harmonic, around 540 Hz, before and after resampling. It can be seen that the smearing of frequency peaks in the spectrum due to speed variation, is greatly reduced after resampling. Only one peak remains at a multiple of the fundamental shaft speed frequency.

Now that the frequencies in the spectrum are more pronounced, automatic cepstral editing is performed on the signal in order to remove the deterministic content of the resampled signal as much as possible. The ACEP method described in section 2.3 is used and the results on the spectrum of the damaged data of the AN7 sensor is shown in Fig. 9a. The damaged data exhibited very prominent shaft speed harmonics and due to the difficulty in properly displaying the total amount of reduction of harmonic content in a spectrum, a graph of the first 100 shaft speed harmonics is presented in Fig. 9b. It can be seen that the ACEP method performs well and is able to reduce these shaft speed peaks by an average of around 13 dB.

The residual signals after ACEP are now used for calculating the envelope spectra. The kurtograms of both the healthy and

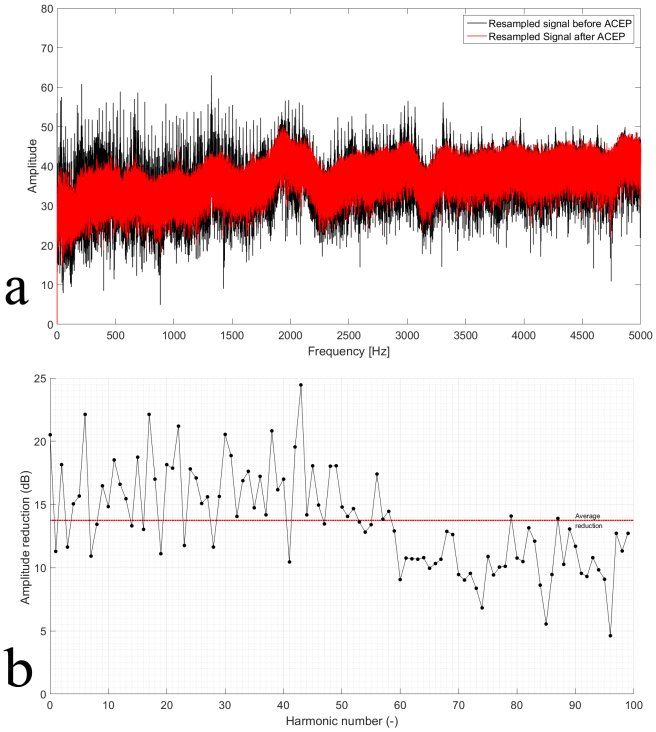

Figure 9. (a) Amplitude spectrum of the AN7 sensor signal before and after ACEP. (b) Graph showing the amplitude reductions, in dB, of the first 100 shaft speed harmonics.

damaged data are generated and examined for differences. Figure. 10 displays the calculated kurtograms and here it can be seen that there is an increase in kurtosis around 13,2 kHz. First however, the normalized envelope spectra of the healthy and damaged data is examined without the use of the kurtogram, thus without band-pass filtering. The result of this can be seen in Fig. 11a. While the ACEP technique tries to reduce the influence of the shaft speed as much as possible, a prominent peak can still be seen at the high speed shaft fre-

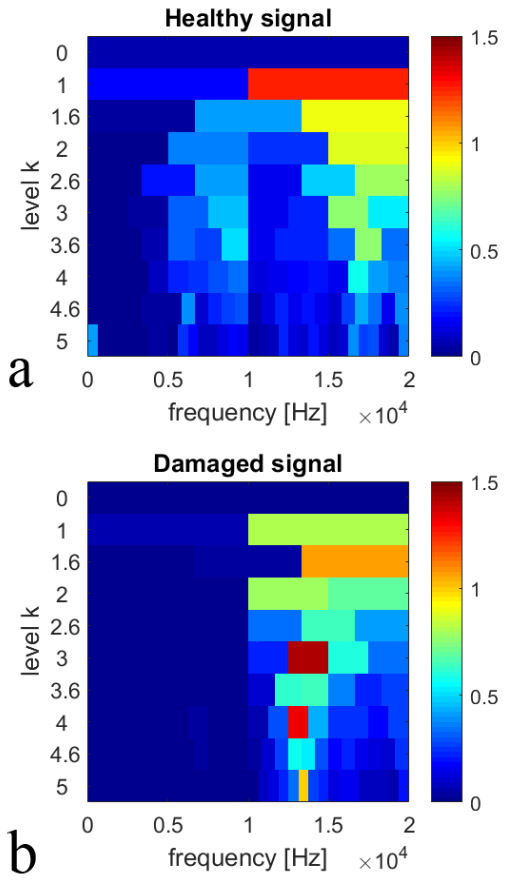

Figure 10. (a) Kurtogram of the healthy AN7 sensor data. (b) Kurtogram of the damaged AN7 sensor data.

quency (*1xHSS*) in the envelope spectrum. This is explained by the fact that ACEP only removes additive components and not modulating ones. Multiple peaks at harmonics of 345 Hz can be observed for the healthy as for the damaged data. The fundamental 345 Hz peak is close to the 2nd harmonic of the sun gear mesh frequency and the 46nd harmonic of the intermediate shaft speed frequency, but isn't an exact multiple of one of these frequencies. Since this component is so prominently present after cepstral editing, it is concluded that the peak in the healthy and damaged data corresponds to the inner race defect frequency or BPFI of the high-speed downwind bearings, which is theoretically around 345.29 Hz for a shaft speed of 30 Hz. This is supported further by the presence of harmonics of the BPFI in the envelope spectrum. The very small difference in frequency between the healthy and damaged data is explained by the slightly lower shaft speed for the healthy data compared to the damaged data. Based on these envelope spectra, it appears that the inner race damage was already present in the baseline healthy data. This is supported by the report of (Sheldon, Mott, Lee, & Watson, 2014), where it is stated that the damage was already present at the time of assembly.

While the gear faults aren't the focus of this paper, it is noted that in Fig. 11a, the envelope spectrum displays a high value at 661 Hz for the damaged data. This corresponds to the gear mesh tooth passing frequency (*GMF*) of the intermediate-speed shaft (ISS) with the high-speed shaft. In the damage report it was later verified that the ISS gear exhibited corrosion, scuffing and wear.

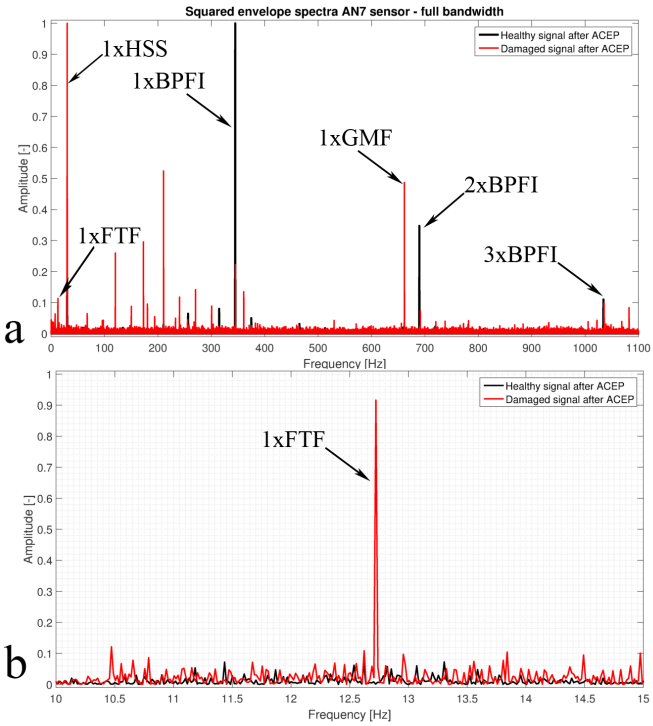

Figure 11. (a) Envelope spectrum generated without the use of filters/kurtogram, indicating the presence of the BPFI & FTF of the high-speed downwind bearings (HSS-B& C). (b) Zoom of the envelope spectrum around the FTF frequency for the healthy and damaged signals after applying ACEP.

The next analysis step makes use of band-pass filtering, based on the info portrayed by the kurtogram. Figure 11b shows a zoom of the envelope spectrum of the residual signal after band-pass filtering. Examination of the spectrum reveals a high peak around 12.71 Hz, which corresponds to the fundamental train frequency (FTF) of the high-speed downwind bearings. Figure 11b shows a clear increase of this frequency in the damaged data compared to the healthy data. Finally, as can be seen in Fig. 11a, the modulation by the 30 Hz shaft speed has increased significantly. This can indicate a possible high-speed shaft imbalance or misalignment or it can be associated with the BPFI modulation of the HSS-B&C bearings. However, the presence of imbalance was later corroborated by the damage report so it is most likely the combination of the two mentioned faults.

In order to demonstrate the effect of the ACEP procedure on

the envelope spectrum, the damaged data is investigated before and after applying cepstral editing. Figure. 12a shows the envelope spectrum of the damaged data of the AN7 sensor before and after cepstral editing and without band-pass filtering. The spectrum before ACEP exhibits far more harmonic peaks, making it difficult to assess possible bearing faults. Added to this, these harmonics mask the presence of bearing faults, as is shown in Fig. 12b. The BPFI of the HSS downwind bearings cannot be detected here before cepstral editing.

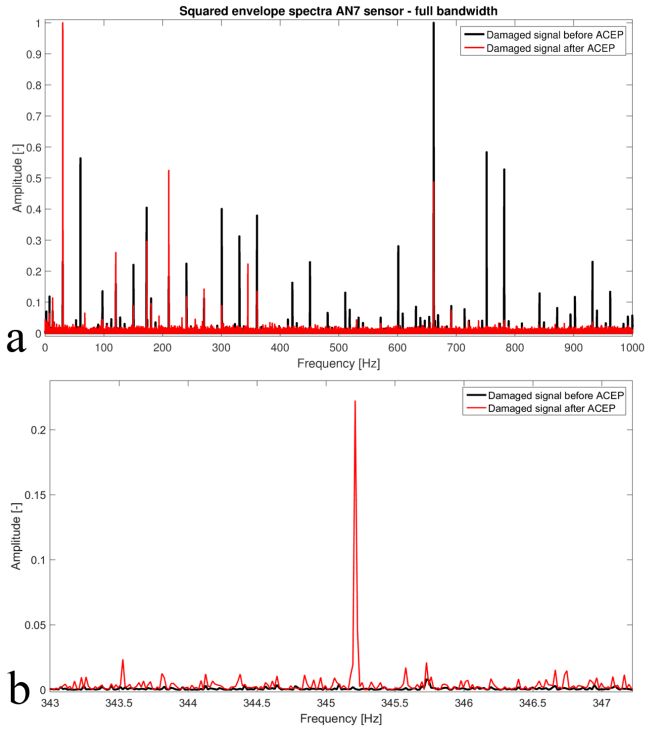

Figure 12. (a) Envelope spectrum of damaged data before (*black line*) and after ACEP (*red line*). (b) Zoom of envelope spectrum around 345 Hz, the BPFI frequency of the high-speed downwind bearings, before and after ACEP.

Intermediate-speed shaft downwind bearings

The analysis procedure followed for the other bearings is similar to the one explained for the high-speed bearings. To reduce the amount of figures, only the resulting envelope spectra are shown. As such, the analysis of the AN6 sensor, which is located close to the intermediate-speed shaft (ISS), is investigated for possible ISS bearing faults. After resampling and cepstral editing, the envelope spectrum for the damaged case, shown in Fig. 13, exhibits clear peaks at even harmonics of the BPFO(105.25 Hz) of the ISS-B&C bearings. It does not however offer clear indications of the fundamental defect frequency itself. This could imply that there are multiple point defects on the bearings, introducing cancellation and reinforcement of components which can modify the appearance of the envelope spectrum (McFadden & Smith, 1985). The damage report confirms this and describes multiple dents, assembly damage and plastic deformation of the ISS downwind bearings. A zoom of the second BPFO harmonic can be seen in Fig. 14 and illustrates the increase in amplitude of this frequency compared to the healthy case.

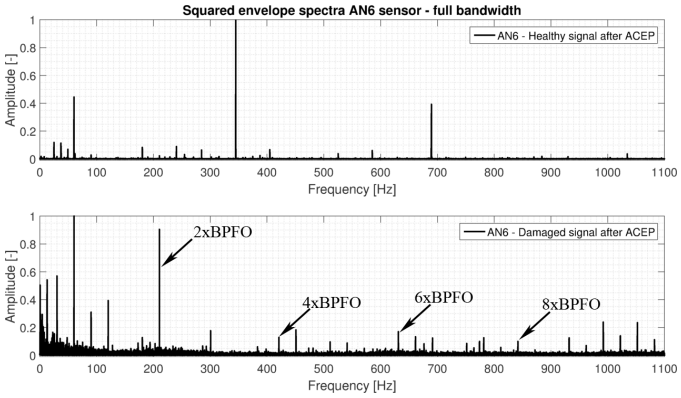

Figure 13. Envelope spectrum of AN6 acceleration signal after resampling and ACEP for the healthy case (*above*) and damaged case (*below*).

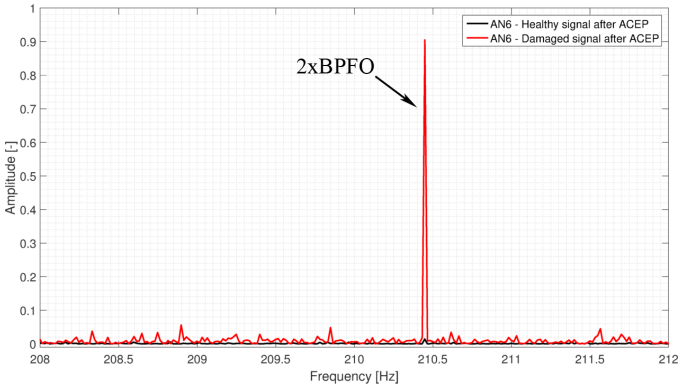

Figure 14. Zoom of envelope spectrum of AN6 acceleration signal around the second BPFO harmonic of the ISS-B&C bearings for the healthy case (*black*) and damaged case (*red*).

Intermediate-speed shaft upwind bearing

Damage was also reported for the ISS upwind bearing and evidence of this was found by using the kurtogram to define a suitable band-pass filter for the envelope analysis. By constructing a band-pass filter with a center frequency of 8759 Hz and bandwidth 2502 Hz, the envelope spectrum in Fig. 15 was generated. A high peak can be seen at 72.94 Hz, which is close to the theoretical BPFI of 73.7 Hz for the ISS upwind bearing. The slight deviation of the theoretical value is

likely due to slip of the roller elements. While this component was quite prominently present in the AN6 and AN7 data set, it is easily mistaken for the second harmonic of the gear mesh tooth passing frequency of the planet gears, which is 73.05 Hz. However, due to it's presence after ACEP and the small frequency difference, it can be concluded that it is in fact the BPFI of the ISS upwind bearing.

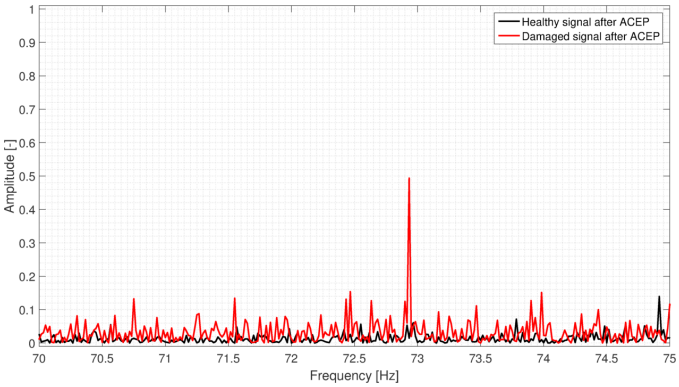

Figure 15. Zoom of envelope spectrum around 72.94 Hz, the BPFI of the ISS upwind bearing, after band-pass filtering with center frequency 8759 Hz and bandwidth 2502 Hz.

Planet carrier upwind bearing

A similar approach as for the ISS-A bearing is used for detecting the 8,8Hz outer race defect frequency of the planet carrier upwind bearing (PLC-A). Again, the BPFO frequency is found through the use of the kurtogram. A band-pass filter with center frequency 24395 Hz and bandwidth 3754 Hz is defined and a zoom of the resulting envelope spectrum is shown in Fig. 16. While the damage report does state that there was fretting corrosion present on the PLC upwind bearing, the corresponding frequency peaks are relatively small and difficult to detect. The partners who participated in the wind turbine gearbox condition monitoring round robin study confirmed this observation as well. Almost no one of the partners was successful in detecting this damage blindly and from Fig. 16a it can be understood why.

5. CONCLUSION

This paper assesses the performance of the automated cepstral editing procedure (ACEP) for a real-world example, more in particular for the data provided by the *National Renewable Energy Laboratory* (NREL). This data was made available in the context of the *wind turbine gearbox condition monitoring round robin study* and is very well documented. Other research teams investigated this data as well, providing an interesting and useful background for comparison of the obtained results. First, the ACEP technique is explained together with other techniques, such as order tracking, band-pass filtering

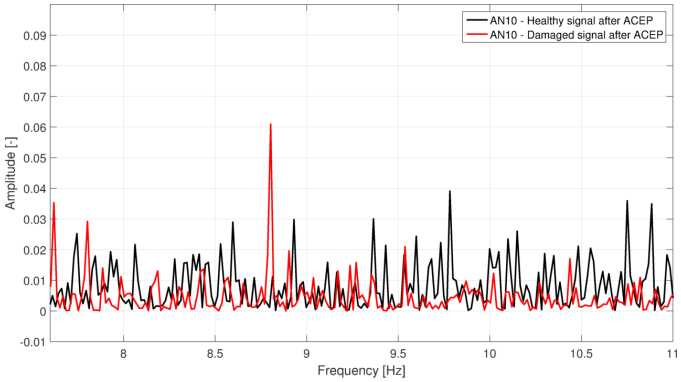

Figure 16. Zoom of the envelope spectrum around 8.86 Hz, the BPFO of the PLC upwind bearing, after band-pass filtering with center frequency 24395 Hz and bandwidth 3754 Hz.

based on kurtosis and enveloping. Second, the performance of the described methods is validated on the NREL data set by examining the sensor acceleration signals for bearing fault frequencies. While the mentioned bearing frequencies are deemed detectable through vibration analysis, the fault frequencies originating from bearings mounted on the lower speed shafts were more difficult to detect than those on the high-speed shaft. Although it isn't the focus of this paper, high values for some of the gear fault frequencies were observed as well in the generated envelope spectra. In summary, the cepstrum editing procedure proved to be a very helpful tool in filtering out the influence of the deterministic content and increasing the sensitivity of the envelope analysis for bearing faults.

6. ACKNOWLEDGEMENT

The authors would like to sincerely thank the National Renewable Energy Laboratory for providing the well-documented data sets and for organizing the wind turbine gearbox condition monitoring round robin study, which produced a lot of interesting and priceless research content. Lastly, we would like to thank the agency for Innovation by Science and Technology for supporting the SBO HYMOP project.

NOMENCLATURE

$BPFO$	Ball Pass Frequency of Outer race
$BPFI$	Ball Pass Frequency of Inner race
FTF	Fundamental Train Frequency
BSF	Ball Spin Frequency
LSS	Low-Speed Shaft
ISS	Intermediate-Speed Shaft
HSS	High-Speed Shaft
CRB	Cylindrical Roller Bearing
$fcCRB$	full-complement Cylindrical Roller Bearing
TRB	Tapered Roller Bearing
A	Upwind
$B\&C$	Downwind
PLC	Planet carrier
$ACEP$	Automated Cepstrum Editing Procedure
$NREL$	National Renewable Energy Laboratory
DTF	Dynamometer Test Facility
SS	Spectral Subtraction
FFT	Fast Fourier Transform
$IFFT$	Inverse Fast Fourier Transform
E	Expectation operator
std	Standard deviation operator

REFERENCES

A.I.Technologies, A. I. (2009). Lubricant failure = bearing failure. *Machinery Lubrication Magazine*(1).

Antoni, J. (2007). Fast computation of the kurtogram for the detection of transient faults. *Mechanical Systems and Signal Processing*, *21*(1), 108–124.

Antoni, J., Daniere, J., & Guillet, F. (2000). Blind identification of nonminimum phase systems using the mean differential cepstrum. In *Signal processing conference, 2000 10th european* (pp. 1–4).

Antoni, J., & Randall, R. (2003). A stochastic model for simulation and diagnostics of rolling element bearings with localized faults. *Journal of vibration and acoustics*, *125*(3), 282–289.

Antoni, J., & Randall, R. (2004a). Unsupervised noise cancellation for vibration signals: part i evaluation of adaptive algorithms. *Mechanical Systems and Signal Processing*, *18*(1), 89–101.

Antoni, J., & Randall, R. (2004b). Unsupervised noise cancellation for vibration signals: part ii a novel frequency domain algorithm. *Mechanical Systems and Signal Processing*, *18*(1), 103–117.

Bogert, B. P., Healy, M. J., & Tukey, J. W. (1963). The quefrency alanysis of time series for echoes: Cepstrum, pseudo-autocovariance, cross-cepstrum and saphe cracking. In *Proceedings of the symposium on time series analysis* (Vol. 15, pp. 209–243).

Boll, S. F. (1979). Suppression of acoustic noise in speech using spectral subtraction. *Acoustics, Speech and Signal Processing, IEEE Transactions on*, *27*(2), 113–120.

Borghesani, P., Pennacchi, P., Randall, R., Sawalhi, N., & Ricci, R. (2013). Application of cepstrum prewhitening for the diagnosis of bearing faults under variable speed conditions. *Mechanical Systems and Signal Processing*, *36*(2), 370–384.

Childers, D. G., Skinner, D. P., & Kemerait, R. C. (1977). The cepstrum: A guide to processing. *Proceedings of the IEEE*, *65*(10), 1428–1443.

Cohen, R. (2012). Signal denoising using wavelets. *Project Report, Department of Electrical Engineering Technion, Israel Institute of Technology, Haifa*.

Courrech, J., & Gaudet, M. (1998). Envelope analysis-the key to rolling-element bearing diagnosis. *Brüel & Kjær Application Notes*.

Dalpiaz, G., Rubini, R., D'Elia, G., Cocconcelli, M., Chaari, F., Zimroz, R., ... Haddar, M. (2013). Advances in condition monitoring of machinery in non-stationary operations. In *Proceedings of the third international conference on condition monitoring of machinery in non-stationary operations cmmno.*

Donoho, D. L., & Johnstone, J. M. (1994). Ideal spatial adaptation by wavelet shrinkage. *Biometrika*, *81*(3), 425–455.

Graney, B. P., & Starry, K. (2012). Rolling element bearing analysis. *Materials Evaluation*, *70*(1), 78.

Ho, D., & Randall, R. (2000). Optimisation of bearing diagnostic techniques using simulated and actual bearing fault signals. *Mechanical systems and signal processing*, *14*(5), 763–788.

Kamath, S., & Loizou, P. (2002). A multi-band spectral subtraction method for enhancing speech corrupted by colored noise. In *Ieee international conference on acoustics speech and signal processing* (Vol. 4, pp. 4164–4164).

Kilundu, B., Ompusunggu, A. P., Elasha, F., & Mba, D. (2014). Effect of parameters setting on performance of discrete component removal (dcr) methods for bearing faults detection. In *Proceedings of the european conference of the prognostics and health management (phm) society, nantes (france), 8th-10th july.*

Lebart, K., Boucher, J.-M., & Denbigh, P. (2001). A new method based on spectral subtraction for speech dereverberation. *Acta Acustica united with Acustica*, *87*(3), 359–366.

Martin, R. (1994). Spectral subtraction based on minimum statistics. *power*, *6*, 8.

McFadden, P., & Smith, J. (1985). The vibration produced by multiple point defects in a rolling element bearing. *Journal of sound and vibration*, *98*(2), 263–273.

McFadden, P., & Toozhy, M. (2000). Application of synchronous averaging to vibration monitoring of rolling element bearings. *Mechanical Systems and Signal Processing*, *14*(6), 891–906.

Ompusunggu, A. P. (n.d.). Automated cepstral editing procedure (acep) as a signal pre-processing in vibration-based bearing fault diagnostics.

Pasti, L., Walczak, B., Massart, D., & Reschiglian, P. (1999). Optimization of signal denoising in discrete wavelet transform. *Chemometrics and intelligent laboratory systems*, *48*(1), 21–34.

Polydoros, A., & Fam, A. T. (1981). The differential cepstrum: definition and properties. In *Proc. ieee int. symp. circuits syst* (pp. 77–80).

Randall, R., & Hee, J. (1982). Cepstrum analysis. *Wireless World*, *88*, 77–80.

Randall, R., Sawalhi, N., & Coats, M. (2011). A comparison of methods for separation of deterministic and random signals. *International Journal of Condition Monitoring*, *1*(1), 11–19.

Randall, R. B. (2011). *Vibration-based condition monitoring: industrial, aerospace and automotive applications*. John Wiley & Sons.

Randall, R. B. (2013). A history of cepstrum analysis and its application to mechanical problems. In *International conference at institute of technology of chartres, france* (pp. 11–16).

Randall, R. B., Antoni, J., & Chobsaard, S. (2001). The relationship between spectral correlation and envelope analysis in the diagnostics of bearing faults and other cyclostationary machine signals. *Mechanical systems and signal processing*, *15*(5), 945–962.

Randall, R. B., & Sawalhi, N. (2011). A new method for separating discrete components from a signal. *Sound and Vibration*, *45*(5), 6.

Randall, R. B., & Sawalhi, N. (2014). Cepstral removal of periodic spectral components from time signals. In *Advances in condition monitoring of machinery in non-stationary operations* (pp. 313–324). Springer.

Sawalhi, N., & Randall, R. (2011). Signal pre-whitening using cepstrum editing (liftering) to enhance fault detection in rolling element bearings. In *Proceedings of the 24 international congress on condition monitoring and diagnostic engineering management (comadem2011), may* (pp. 330–336).

Sawalhi, N., & Randall, R. B. (2004). The application of spectral kurtosis to bearing diagnostics. In *Proceedings of acoustics* (pp. 3–5).

Sheldon, J., Mott, G., Lee, H., & Watson, M. (2014). Robust wind turbine gearbox fault detection. *Wind Energy*, *17*(5), 745–755.

Sheng, S. (2012). Wind turbine gearbox condition monitoring round robin study–vibration analysis. *Contract*, *303*, 275–3000.

BIOGRAPHIES

Cédric Peeters was born in Lier, Belgium, in 1992. He received his bachelor's degree in mechanical and electrical engineering in 2013 from the KU Leuven. During 2014-2015 he wrote his master-thesis and received his master's degree at KU Leuven in mechanical engineering, specialisation automotive engineering, in june 2015. Currently his time and effort goes into his PhD, concerning vibration-based condition monitoring.

Patrick Guillaume was born in Anderlecht, Belgium, in 1963. He received the degree in mechanical-electrotechnical engineering in 1987 from the Vrije Universiteit Brussel, Belgium. In 1987 he joined the Department of Electrical Engineering (ELEC) of the Vrije Universiteit Brussel and received the Ph.D. degree in 1992. In 1996 he joined the Department of Mechanical Engineering (WERK) where he is currently lecturer. His main research interests are situated in the field of system identification, signal processing and experimental modal analysis.

Jan Helsen was born in Antwerp, Belgium, 1983. He received his master in Engineering Sciences specialisation Mechatronics at KU Leuven. In 2006-2007 he wrote his Master-Thesis during a research stay at BMW R&D Munich. From 2007-2012 he joined the KU Leuven department of Mechanical Engineering for his PhD titled: The dynamics of high power density gearboxes with special focus on wind turbines. From 2012-2014 Jan initiated his current topic focussing on monitoring of wind turbine drivetrains in cooperation with ZF Wind Power and Siemens in the framework of an IWT Innovation Mandate. Currently Jan is post-doc within the Brussels Wind Energy Research Institute, BruWind.